



Tuning the surface morphology of self-assembled graphene-like thin films through pH variation



Michela Alfè^a, Valentina Gargiulo^a, Roberto Di Capua^{b,*}

^a Istituto di Ricerche sulla Combustione, Consiglio Nazionale delle Ricerche (IRC)-CNR, p.le V. Tecchio, 80, 80125 Napoli, Italy

^b Dipartimento di Fisica, Università di Napoli "Federico II", and CNR-SPIN UOS-Napoli, via Cintia, 80126 Napoli, Italy

ARTICLE INFO

Article history:

Received 22 February 2015

Received in revised form 19 June 2015

Accepted 19 June 2015

Available online 24 June 2015

Keywords:

Graphene-like (GL) layers

Zeta potential

pH

AFM

ABSTRACT

Graphene-like (GL) layers were prepared through a two steps oxidation/reduction method starting from a high surface carbon black, and pH of the GL layers in water suspension was varied. The effect of pH of such suspension on the morphology of self-assembled GL films has been studied. Zeta potentials of the water suspensions were measured to estimate the stability of the suspension at several pH values and to select the samples for deeper investigation by atomic force microscopy (AFM). AFM measurements on four different samples are then described and discussed. The reported results show how the surface roughness and morphology are affected by the pH in the preparation process: in particular, the lowest pH sample exhibits a granular surface, while at higher pH more regular morphologies are produced, with interesting observations as concerns the thickness of some surface features. The observations are interpreted in terms of the forces acting in water suspension and of the role of hydrophobic or hydrophilic behaviors. The results demonstrate the possibility to tune the surface properties of GL films by simply acting on the pH of the suspension during the fabrication, and help to understand the microscopic physical mechanisms involved in the film assembly.

© 2015 Elsevier B.V. All rights reserved.

1. Introduction

The rapid development and upgrading of optoelectronic devices (liquid crystal displays, organic light emitting diodes, organic photovoltaic cells and touch panels) has induced a growing demand of transparent conductive films. Films have to be conductive and transparent but also flexible, cheap, and compatible with large scale manufacturing methods (current optoelectronic devices are normally assembled on hard substrates such as glass) [1]. Organic π -conjugated molecules (aromatic hydrocarbons as acenes and fused arenes and substituted derivatives) have attracted great attention in nanodevices fabrication [2,3] due to the presence of delocalized electrons inside their structure, which offer the development of proper conductive pathways. Numerous reports addressing the use of carbon nanotubes, reduced graphite oxide and graphene thin films as ideal transparent electrodes for optoelectronic devices have appeared in the past years [4–6]. Carbon-based films address a broad range of coating applications [7], and some

recent studies showed their possible applications for medical applications [8], and photocatalysis [9,10].

The production of carbon-based films simultaneously with high stability, controlled thickness, and tunable performances still remains an interesting challenge. The set-up of versatile and inexpensive coating methods for the deposition of carbon-based films with controllable morphology and thickness is still a goal in materials science research.

A new approach for producing graphene-like (GL) thin films has been recently reported [11]. In the proposed method GL layers were produced in mild conditions and in aqueous environments with high yields (55% mass yield) through a two steps oxidation/reduction method starting from a nanostructured carbon black (CB). The proposed approach for making GL thin films is environmentally advantageous because all procedures are performed in aqueous media, and it is highly compatible to an industrial scale-up process. Thanks to their good stability in water, driven by residual oxygen functional groups on the GL layers edge, GL appears as a very versatile nanomaterial, suitable for the preparation in aqueous environment of composites with tunable chemical/physical properties such as microporosity, conductivity, catalytic performances and biocompatibility [12–14].

The GL layers undergo to self-assembling in thin film on surfaces after drying, as shown by transmission electron microscopy

* Corresponding author. Tel.: +39 081676915.

E-mail address: roberto.dicapua@na.infn.it (R. Di Capua).

and atomic force microscopy (AFM) [11], thanks to the instauration of hydrophobic interactions between the graphenic layers, as typically observed in reduced graphite oxide [15].

For a convenient exploitation of the process and film thickness control it is fundamental to carefully explore each aspect of the film preparation. Due to the residual functional groups on the GL layers edge, the quality of the thin film is expected to be strongly dependent on the pH of the graphene-like layers suspension. This study clarifies the effect of the pH on the graphene-like film quality and its capability in determining the surface properties, and introduces a simple picture of the process to describe the involved physical mechanisms.

2. Materials and methods

2.1. Samples preparation

All the chemicals (analytical grade) were purchased from Sigma Aldrich and used as received. Furnace CB type N110 was obtained by Sid Richardson Carbon Co. NaCl and NaOH solutions for potentiometric study were prepared by dissolving the Carlo Erba RPE products in water. NaOH solutions were titrated with HCl stock solutions using a phenolphthalein indicator. HCl stock solution was analyzed by KHCO_3 , using a mixed methyl red–bromocresol green indicator, with a reproducibility of 0.1%.

GL layers in water suspension were obtained through a two steps oxidation/reduction method [11] starting from a CB. Briefly, 500 mg of CB powder (15–20 nm primary particles diameter, specific BET area $139 \text{ m}^2/\text{g}$) was oxidized with 10 mL of nitric acid (67 wt.%) at 100°C under stirring for 90 h. The oxidative step destroys the CB backbone providing hydrophilic nanoparticles functionalized with oxygen functional groups (mainly carboxylic). This treatment affects the edge of the CB graphitic layers leaving untouched the basal plane. The oxidized carbon nanoparticles were recovered by centrifugation and washed until acid traces were successfully removed. Following the oxidation step, the nanoparticles (20 mg) were dispersed in 20 mL distilled water and treated with $450 \mu\text{L}$ of hydrazine hydrate (50%) at 100°C under reflux for 24 h. This treatment reduces the hydrophilic character of the nanoparticles and promotes self-assembling phenomena as a consequence of the hydrophobic interaction between the graphitic planes [11]. At the end of the reaction the excess of hydrazine was neutralized with nitric acid (4 M). The solid was washed with distilled water, recovered by centrifugation (3000 rpm, 30 min) three times in order to remove traces of unreacted reagents and acid and named GL layers. The pH of the as-prepared GL layers water suspension was 3.70. The dried GL layers are insoluble in water and in the most common organic solvents, both polar and apolar (ethanol, N-methylpyrrolidinone, dichloromethane, heptane, dimethylformamide).

2.2. Characterization procedure

The determination of GL layers surface acidic functionalities was performed adapting the test reported by Visentin et al. [16] for oxidized carbon nanotubes. The total amount of GL layers used for each assay was estimated to be 0.01 mg. GL layers water suspensions were treated with an ethanolic solution of thionin acetate (THA, 1.5 mL, $4.3 \mu\text{M}$) for 30 min with constant stirring at room temperature. The suspension was filtered using a $0.02 \mu\text{m}$ Anotop 25 filter (Whatman), and the absorbance was measured at 604 nm [17] with a HP 8453 Diode Array spectrometer. The THA that had not interacted with the material was estimated through a calibration curve. The total amount of THA that had interacted with the GL was estimated and corrected for the unspecific interaction by subtracting

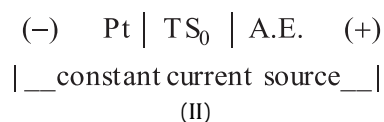
the amount of THA interacting with a reference carbonaceous material (CB) exhibiting no acidic functionalities ($5.28 \times 10^{-2} \text{ mmol/g}$). The quantification of the acidic sites was performed by considering a 1:1 stoichiometry between the cationic THA and the carboxylic functionalities.

The acid–base behavior of the carboxylic functional group on surface of GL layers has been studied in NaCl 0.25 M, measuring the potential of a glass electrode sensitive to proton activity. The interval of pH investigated was $2.7 < \text{pH} < 7$. The glass membrane electrodes as well as the automatic burettes “640 Multi Dosimat” were supplied by Metrohm. Measurements were carried out into an air thermostat. The temperature was kept at $25.00 \pm 0.02^\circ\text{C}$ (measured using a Pt100 TERSID thermocouple). Coulometric variations of the solution composition have been carried out using a Hewlett Packard DC Power Supply. The current intensity was accurately determined by reading the potential drop at the ends of a calibrated resistance coil, connected in series to the coulometric device.

The study was performed by measuring the electromotive force (Emf) of the cell (I):



in which G.E. indicates a glass membrane electrode reversible to protons; R.E. is an external reference electrode, connected to test solution (TS) through a salt bridge. In the first step the cell constant ($^*\text{Eg}$) and the initial number of micromoles of H^+ (n_0) were determined. A coulometric–potentiometric titration was then performed: a weighed volume V_0 (50.00 cm^3) of a solution $\text{TS}_0 = 0.25 \text{ M}$ NaCl was introduced into the measuring vessel. The hydrogen ion concentration, h , was coulometrically varied by means of the circuit (II):



where A.E.: 0.25 M NaCl/HgO(s)/Hg(s)(Pt) is an external auxiliary electrode, connected to TS_0 through a salt bridge and Pt denotes a platinum electrode. In order to estimate the amount of electrolysis produced by circuit (II), according to reaction $2\text{H}_2\text{O}(l) \rightarrow 4\text{H}^+(\text{aq}) + 4\text{e}^- + \text{O}_2(\text{g})$, after each delivery of current of intensity $i(A)$, for a time $t(s)$, the Emf of cell (II), $E(\text{mV})$, was measured until constancy. The Nernst potential of cell (I), E , can be written as in Eq. (1):

$$E = ^*\text{Eg} + 59.16 \log h + E_j \quad (1)$$

where $^*\text{Eg}$ is the glass electrode constant and h represents the equilibrium concentration of protons. For acidities, h , lower than 10^{-3} M , the junction potential E_j , can be neglected. Similarly, the term accounting for the activity factor changes can be also neglected, because the composition of TS does not differ appreciably from that of the ionic medium. According to Faraday’s law, the number of micromoles of produced H^+ ions, μ , is numerically equal to the microfaradays generated by the circuit (II), as written in the Eq. (2):

$$\mu = \frac{(i * t)}{0.096487} \quad (2)$$

The sets of experimental data (Eg , μ) can be further transformed into a linear function, i.e. a Gran plot [18], which provides the value of n_0 , as well as E_0 , that are indispensable for the next step.

A potentiometric–volumetric titration of 0.250 g of sample in NaCl 0.25 M has been carried out. Titration was performed by stepwise additions, by means of an automatic buret issuing volumes V_T of NaOH or HCl stock solutions.

The experimental data (Eg, V_T) were interpreted by the software LETAGROP-ETITR [19].

The zeta potentials of the GL suspensions were measured using a Malvern Zetasizer Nano ZS instrument. The zeta potential measurements were performed at a GL concentration of 0.05 mg/mL as a function of pH in the 2–12 pH range. Each point of pH was reached by adding 100 μ L of NaOH 0.1 M to the GL layers suspensions and then by subsequent additions of the proper amount of HCl (0.1 M). The pH and the zeta potential measurements were performed after the time necessary for the pH stabilization (approximately 1 h under continuous stirring).

Samples for AFM imaging were prepared by drop-casting the GL suspensions onto freshly cleaved mica substrates (grade V-1, Electron Microscopy Sciences) which were then allowed to dry in air. AFM images were taken by means of an XE100 Park instrument operating in noncontact mode (amplitude modulation, silicon nitride cantilever from Nanosensor) at room temperature and in ambient conditions.

X-ray photoemission spectroscopy (XPS) was performed in a ultra high vacuum chamber (base pressure of 1×10^{-10} mbar) equipped with a Specs Phoibos 150 electron analyzer, using Al K_{α} (photon energy: 1486.6 eV) X-ray source.

3. Results and discussion

GL layers in water suspension consist of small flat nanoparticles decorated at the edge with oxygen-containing groups (mainly carboxylic/carboxylic and hydrazones) with graphenic basal plane untouched [11]. The amount of carboxylic groups estimated by the modified THA method resulted to be 0.16 mmol_{COOH}/g, lower with respect to the amount estimated for the unreduced GL layers (0.46 mmol_{COOH}/g).

The functional groups on the surface of GL were also investigated by coulometric–potentiometric titration in the pH range $2.7 < \text{pH} < 7$. Two functional groups on the surface in the carboxylate region (pK_a 2.0–5.0) [20] with $\text{pK}_a = 3.40 \pm 0.05$ (number of sites = 900 ± 30 mmol/g) and $\text{pK}_a = 5.5 \pm 0.1$ (number of sites = 240 ± 30 mmol/g) respectively, have been identified. The higher pK_a value (5.5) is ascribable to the presence of lactones and carboxylic anhydride groups that tend to hydrolyze in the presence of acids and bases [21]. It is noteworthy that the number of sites attributable to carboxylic acid sites is significantly higher with respect to the value estimated by the THA method and more consistent with literature data referring to related materials such as graphite oxide [22]. This discrepancy can be rationalized considering that the method with THA, optimized for the detection of low concentration of carboxylic sites ($\sim 10^{-2}$ mmol/g) as typically detected on carbon nanotubes [16] and soot after reaction with hydroxyl radicals ($\sim 10^{-4}$ mmol/g [17]), probably fails when applied to nanomaterials featuring a more dense distribution of carboxylic sites due to the steric hindrance of THA.

The stability of the GL layers water suspensions was evaluated by zeta potential analyses. The measured zeta potentials (Fig. 1) were always negative indicating the presence of partly preserved anionic charge. The zeta potential of the GL dispersion is pH-dependent which is consistent with the fact that the ionization of residuals of carboxylic groups, responsible of the anionic charge, is strongly related to pH. GL was found to be stable in a wide range of pH values, namely 3–12. The zeta potential was below -30 mV when the pH was greater than 2 and it reached -45 mV when the pH approached 12. The zeta potential values lower than -30 mV are conventionally considered as an indication of sufficient mutual repulsion to ensure the stability of dispersions [23]. The films and the effect of the reduction process have been also investigated by Raman spectroscopy and UV–visible spectroscopy, whose

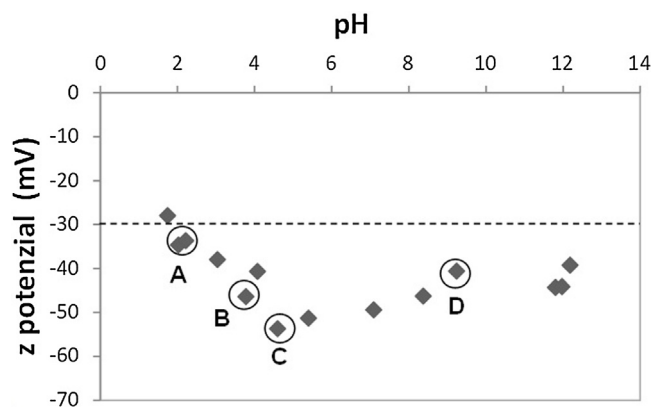


Fig. 1. pH-dependent zeta potential curves of the GL layers suspensions (0.05 mg/mL).

main results are reported elsewhere [11]. Briefly, the shape of the Raman spectra is consistent with the occurrence of a multilayer structure. The comparable height of the D and G bands is indicative of significant structural disorder, while the fact that the D-band to the G-band ratio is nearly the same for the reduced GL layers and the unreduced ones indicates that the oxidation process preserves the presence of the graphitic network being the chemical functionalization at the edge and not at the basal planes of the GL layers. UV–visible spectroscopy confirms the preservation of the graphitic network in the reduction process; furthermore, the spectra collected on them are blue-shifted compared to the ones on CB, indicating a decrease in the size of the π conjugation domains.

Four pH points were selected for a deeper investigation, namely pH 2.0, 3.7, 4.6 and 9.5, which in the following will be indicated as Sample A, B, C, D, respectively. The four samples and pH points correspond to: (1) GL layers in acid suspension at the limit of the stability range of the suspension (pH 2.0, Sample A); (2) as prepared GL layers suspension (pH 3.7, Sample B); (3) GL layers suspension within the limit of the stability range of the suspension (pH 4.6, Sample C); (4) GL layers in basic suspension (pH 9.5, Sample D).

The GL layers water dispersions at the selected pH points were drop-casted at the concentration of 1 mg/mL onto freshly cleaved mica substrates, to ensure an atomically flat substrate, dried at room temperature. Information about the surface features of the films obtained after GL drying were obtained by AFM.

Fig. 2 shows the topographic images acquired on the four investigated samples. All images report a $5 \mu\text{m} \times 5 \mu\text{m}$ scan, acquired in the True Non Contact™ mode of operation of the XE-100 Park system, together with a line profile representative of the surface morphology.

Sample A (Fig. 2a), prepared in acid suspension at the limit of the stability range, exhibits a very rough surface, characterized by the presence of grains having width of the order of one or few hundreds nanometers, which lead to a surface peak-to-peak roughness of about 50–100 nanometers.

On the contrary, the samples prepared in suspensions with higher pH show an extremely different morphology.

The surfaces of both Sample B and Sample C look atomically flat over large areas (Fig. 2b and c). However, on the surface of Sample C, there are some isolated “islands” having different lateral sizes. For statistical comparison, on Sample A the grains result in a root mean square roughness of about 43 nm, while on the collected image on Sample B it is less than 1 Å and on sample C it is about 9 Å.

The selected profile on the largest island on the imaged surface of Sample C shows steps of vertical height slightly more than 4 nm, having the same flatness of the surrounding surface. Such flatness suggests that the observed islands are actually made by the same

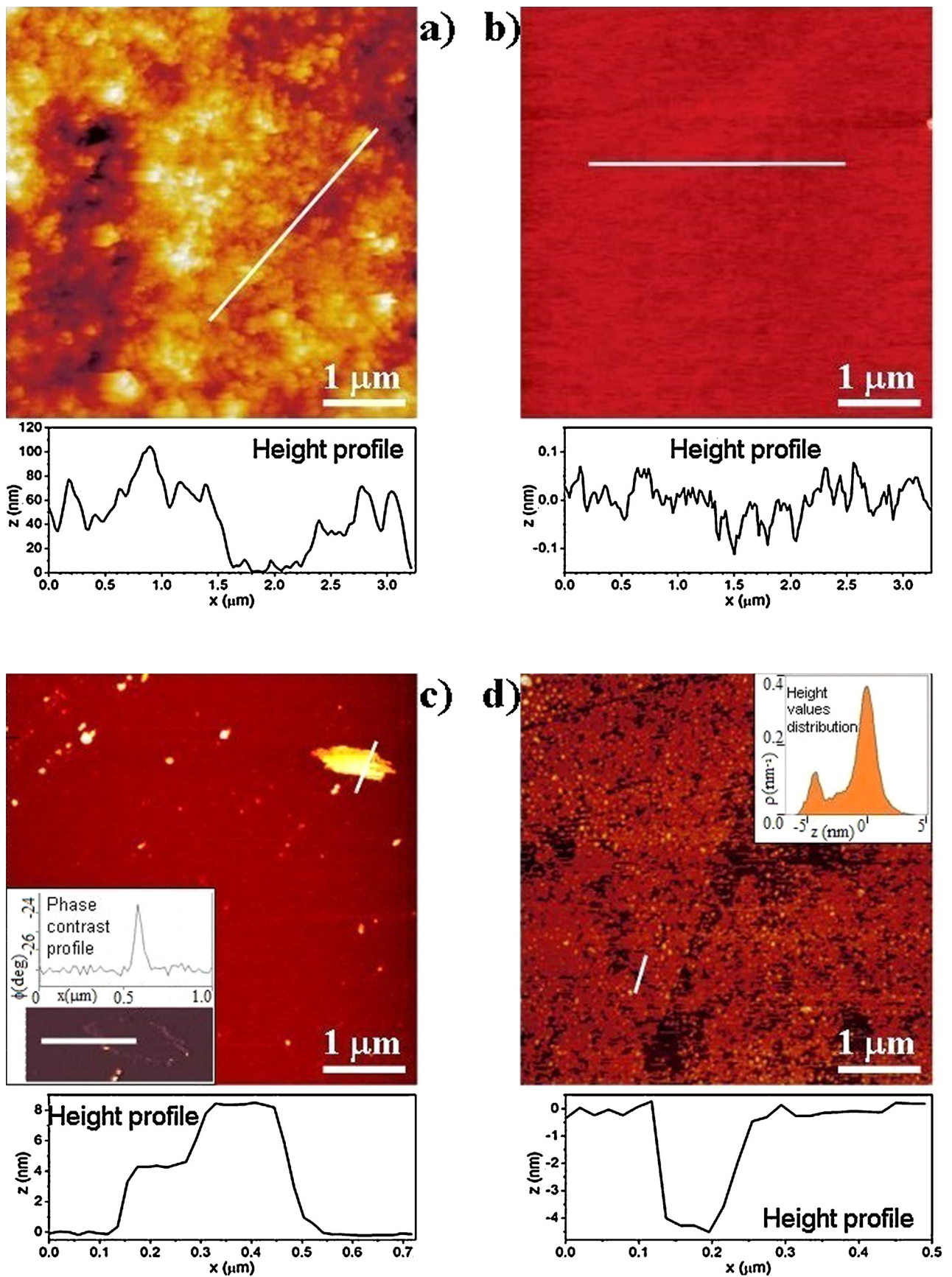


Fig. 2. AFM topographic images with a line profile for each investigated sample; all the reported images correspond to a scan area of $5\ \mu\text{m} \times 5\ \mu\text{m}$. (a) Sample A; (b) Sample B; (c) Sample C (in the inset: the phase contrast profile on a line crossing the large “island” on the top-right of the image); (d) Sample D (in the inset: histogram of the distribution of measured height values on the image).

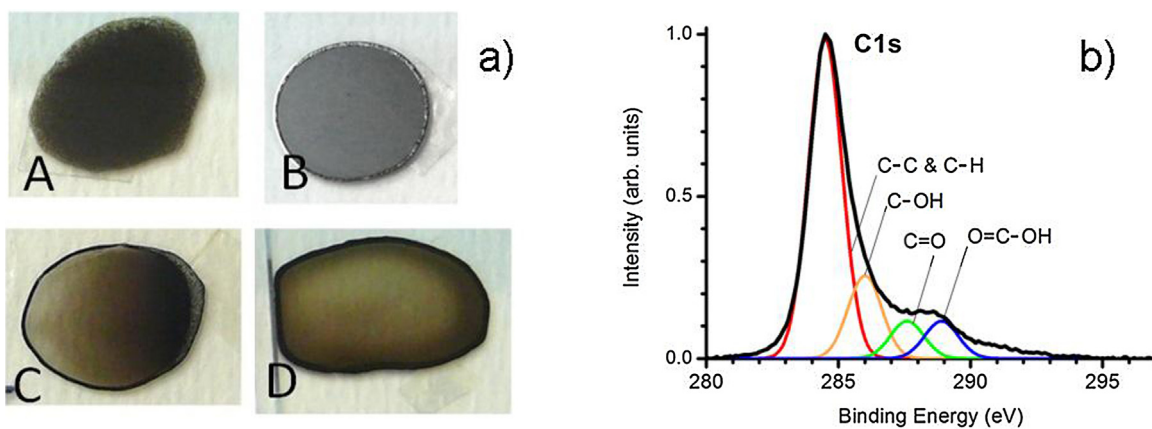


Fig. 3. (a) Images of the drop casted films corresponding to measured Samples A (pH 2.0), B (pH 3.7), C (pH 4.6), D (pH 9.5); (b) C 1s XPS spectrum on GL surface, and its deconvolution in Gaussian shape peaks corresponding to different functional groups.

material as the surrounding carbon surface, and not by spurious phases or unrelated particles. This is confirmed by the phase contrast image: the inset in Fig. 2c shows a phase profile taken across the edge of the island. The phase image in the noncontact AFM scan (repulsive van der Waals regime, amplitude modulated oscillation) is indeed able to provide qualitative information about the chemical nature of the imaged surface, the phase shift of the induced oscillation being sensitive to the chemical functionalities of the surface itself (through differences in the mechanical interaction between the tip and the surface itself). It has been showed on graphene nanosheets produced by chemical reduction of graphene oxide [24] that the different degree of hydrophilicity and hydrophobicity or differently oxidized regions are revealed by a phase upper-shift of the order of 2° – 3° (such phase shifts are well above the sensitivity of our instrument, cf. inset of Fig. 2c). The reported profile shows that no differences are detected between the phase shift on the main surface and on the island.

As concerns Sample D, representative of samples obtained in basic suspension, an “uncompleted” layer appears over an underlying flat surface: the topographic image (Fig. 2d) exhibits regions with lacks in the topmost surface. This circumstance is confirmed by a histogram (in the inset) of the measured relative heights, which form a clearly bimodal distribution. The upper peak is associated to the upmost layer, while the presence of the second peak at a lower value indicates that the holes in this layer have basically the same depth. It is worth to note that the vertical separation between these two layers is between 4 and 5 nm, as shown also in the reported topographic profile. The same value or doubled is measured on the isolated “brighter” spot on the surfaces, also resembling what already described for the surface of Sample C. These observations suggest that the uncompleted layers of Sample D, as well as the large island imaged on the surface of Sample C, could be seeds for further layers. Surprisingly, there is apparently a “fundamental” vertical thickness of more than 4 nm: in Ref. [11], AFM scans on fractured flat graphene-like samples seemed to show steps having the same basic vertical unit.

The trend of the morphological behavior as a function of the pH solution can be interpreted in terms of forces acting into the water suspension and the consequent aggregation processes between GL particles and layers.

The increase of solution pH results in an increase of the charge density driven by the progressive deprotonation of the residual carboxylic functional groups (the carboxylic groups are progressively converted in the anionic form $-\text{COO}^-$). As a consequence, the GL layers have a more hydrophilic character going from Sample A to Sample D, monotonically. The increase of the hydrophilicity makes

the formation of GL–water interfaces energetically favorable, leading to a positive spreading coefficient [25] and to the consequent formation of “wet” GL layers: in other words, the energetically favorable interface formation corresponds to a low surface tension between GL layers and water, and to the consequent tendency to maximize the contact surface. This situation occurs in Samples B, C, D, and the flat layers are formed in the solution. On the contrary, in Sample A, at lower pH, a completely different regime takes place: the surface charge tends to decrease as a consequence of the presence of the carboxylic groups at the edge of the GL layers in the neutral form ($-\text{COOH}$). The result is that GL layers are forced to aggregate to minimize the contact with the polar solvent, producing the grains observed in the AFM image.

A visual inspection of the dried films qualitatively supports our identification of two fluidodynamical regimes. Fig. 3a shows how the films B, C, D, exhibit the so called “coffee ring stain”, characteristic of aqueous colloidal dispersions in which the dispersed material can easily flow through the solution [26]; on the contrary, Sample A has a more uniform aspect, which can be ascribed to the formation of the large observed GL grains.

As concerns the surface chemistry and its role in determining the observed behavior, the presence of residual carboxylic groups is also confirmed by X-ray Photoemission Spectroscopy (XPS) performed on the GL surface. The C 1s XPS spectrum is reported in Fig. 3b. The spectrum has been deconvoluted using Gaussian peak shape. A Shirley background correction has been applied before the deconvolution, and the deconvolution has been performed with each component constrained to have the same full-width at half-maximum (resulting to be 1.5 eV). The C 1s spectrum exhibits the main peak (at a binding energy of about 284.5 eV) corresponding to carbon involved in C–C and C–H bonding, together with the peaks assigned to C–OH, C=O and COOH functional groups. In particular, a strong shoulder at about 289 eV is observed, characteristic of the presence of carboxylic (COOH) groups. Such shoulder is fitted by a Gaussian contribution from carboxylic group with a weight larger than what usually reported in XPS measurements on typical carbonaceous surfaces [27,28], suggesting that, despite the reduction process, there is still a relatively large amount of surface carboxylic functional groups able to drive the surface aggregation in the suspension.

From the point of view of microscopic forces between elementary constituents, the crossover between the two regimes is determined, in the simplest picture, by the competition between van der Waals (vdW) and electrostatic double layer (DL) forces. The vdW attraction exhibits a typical power law as a function of the separation (long range interaction) between charged particles

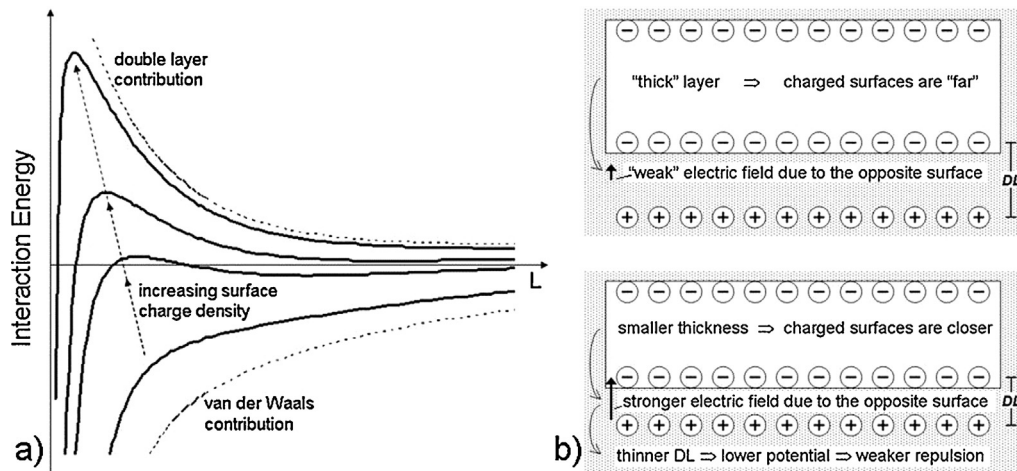


Fig. 4. (a) Qualitative picture of the interaction energy between suspended particles as a function of their separation L , resulting from the combined action of vdW attraction and DL repulsion, for different surface charge density. (b) Sketch of one possible mechanism leading to the formation of GL layers of selected thickness.

in the suspension, while the repulsive DL contribution (it must be specified that the repulsion arising from the DL forces has osmotic/entropic nature, rather than electrostatic) is characterized by an exponential decay vs. separation with a characteristic decay length (short range interaction), the Debye screening length due to the counterions in the solution. Their combined action results in a total particle–particle interaction potential as a function of separation h having a maximum for a given value (typically few nanometers), i.e. a potential barrier which acts against aggregation (Fig. 4a). However, when the particle surface charge approaches zero or when the electrolyte concentration increases above some concentration (*critical concentration coagulation*), and both circumstances occur in our case at lower pH, the DL repulsion has lower intensity and shorter Debye length, so that the vdW attractive force dominates: the potential profile can lose the barrier (it may approach the shape of a pure vdW interaction) and the particles in the suspension can easily coagulate. The surface morphologies observed by AFM indicate that this regime characterizes sample A. In the other samples, the *hydrophilic forces* drive the aggregation process to the surface maximization described above.

In samples B, C, D, an ideal maximization of exposed surfaces would lead to ideal GL monolayers. However, our measurements indicate the formation of thicker layers, having a well defined thickness, i.e. composed by a given number of monolayers. A possible explanation of this interesting phenomenon can be given again in terms of competition between the forces acting into the suspension, but acting between extended flat surfaces instead of small particles. In this picture, the vdW and DL forces (per unit surface, i.e. the pressures) as a function of separation L can be written respectively as [29]:

$$\Pi_{vdW}(L) = \frac{A_H}{6\pi L^3} \quad (3)$$

$$\Pi_{DL}(L) = -\frac{\kappa^2}{2\pi} Z \cdot \exp(-\kappa L) \quad (4)$$

which correspond to interfacial Gibbs free energies per unit area of $-A_H/12\pi L^2$ and $(\kappa/2\pi)e^{-\kappa L}$ respectively. A_H is the Hamaker constant of the trilayer water-GL-water, Z is a constant defining the strength of the DL interaction, κ^{-1} is the Debye screening length. A quantitative evaluation of such forces and related Gibbs energies is well beyond the purposes of this work: in particular, the Z and κ parameters are related in a non-trivial way to the pH of the solution (i.e. to the counterions concentration) and to the charge (or potential) of the charged surfaces (while vdW forces are nearly independent on pH). What one can say, is that our observation

suggests that the vdW/hydrophilic attraction between monolayers drives them to aggregate against DL repulsion.

This simple picture well reconciles the measured morphological trend with the surface deprotonation as a consequence of pH variation. Nevertheless, it cannot yet account for the experimental indication of a selected thickness in the multilayer formation, at the least in Samples C and D: a mechanism depending on the layer thickness (or, equivalently, on the number of aggregated monolayers) must be invoked. We suggest two possible general mechanisms, provided that further experimental work is needed for a conclusive answer.

A first explanation can be given in terms of balance between surface energies of the layers and the aggregation energy (energy required for the crystal formation), similar to what happens in the nucleation of polymers in solutions [30,31]. In this frame, the variation of Gibbs free energy associated to the formation of a layer of average thickness d and surface S can be written as:

$$\Delta G = 2\gamma S - \Delta F S d \quad (5)$$

In the expression above, γ is the surface free energy per unit area (one layer exposes two surfaces of area S), and ΔF is the bulk free energy of crystallization per unit volume (since we observe layer thicknesses much smaller than the lateral sizes, we neglect the contribution of the lateral surface energy). The layer formation is energetically favorable (i.e. the formed layer is stable against disaggregation) if $\Delta G < 0$, which means if:

$$d > \frac{2\gamma}{\Delta F} \equiv d_{\min} \quad (6)$$

The GL layer is stable only over a given minimum thickness d_{\min} (whose value is independent on the surface S); a further aggregation over d_{\min} can be prevented by the arising DL repulsion, at least in Samples C and D, where we observed the preferred thickness and where the DL repulsion can be actually expected to be stronger (according to the trend of the interaction vs. surface charge depicted in Fig. 4a; note that a stronger DL repulsion could also compete with the aggregation process occurring to minimize G , and be therefore responsible of the higher observed “fragmentation” in Samples C and D than in Sample B). Since ΔF and γ are basically related to the material properties and not to the pH (even for γ into the solution: from an energetically point of view, the excess surface charge is compensated by a higher counterion concentration near the surface), this would also be consistent with the fact that the selected thickness is nearly the same in both Sample C and D.

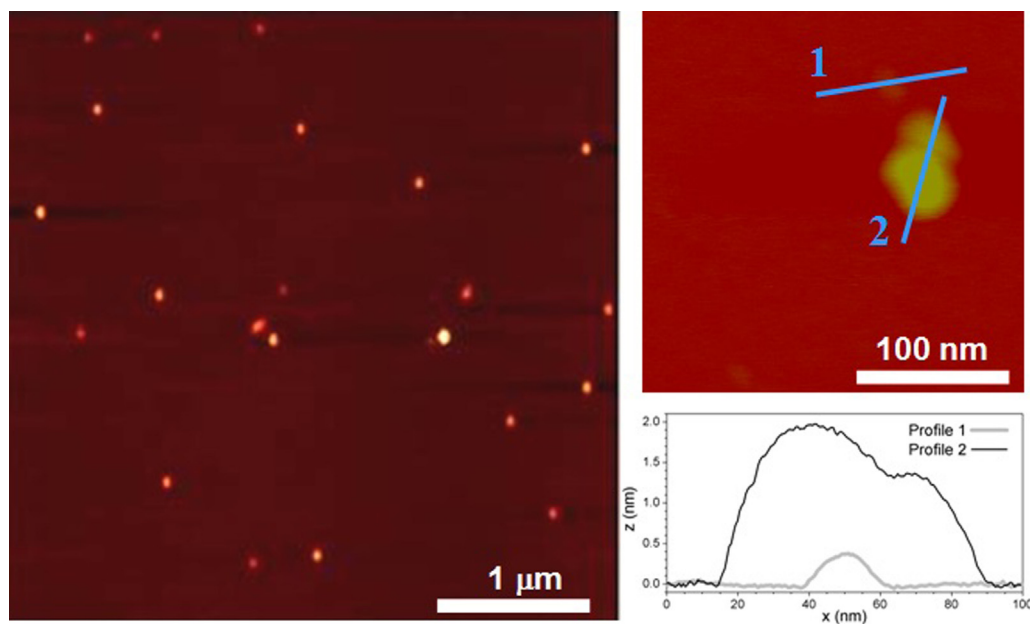


Fig. 5. AFM characterization: NC-AFM topographic images, $4\ \mu\text{m} \times 4\ \mu\text{m}$ and $300\ \text{nm} \times 300\ \text{nm}$, showing the presence of GL nanoparticles on a mica substrate; the profiles taken on some nanoparticles show that such structures have height ranging from less than 1 nm to few nanometers.

Alternatively, a second, thickness-dependent, mechanism can be found taking into account the interaction between the opposite charged surfaces of a layer. The DL properties are usually derived by thinking in terms of an isolated charged surface in an electrolyte. In our case, we have two charged surfaces separated by a thin GL layer: as a consequence, the properties of each DL in such layer are affected by the presence of the charge on the opposite surface. In the simplest electrostatic picture, sketched in Fig. 4b, a “close” opposite charged surface produces a non-negligible electrostatic field whose effect is to narrow the DL thickness; assuming an unchanged surface charge density, this results in a lower DL potential (according to Grahame equation [32]), and therefore in a lower stability against aggregation (as a first intuitive approximation, the DL can be assimilated to an ideal capacitor with constant charge, in which the potential must decrease when the plates approach each other). When a given thickness is reached, this effect is low enough (the field from the opposite surface must be actually seen as a dipole field rather than a solely surface field) to allow the DL repulsion to prevent further layer aggregation.

Finally, we wanted to dissipate the doubt that the observed 4 nm layers are not made by somewhat fundamental constituents, or to an artifact apparent thickness due to the interaction between AFM tip and GL surface (similarly to what observed, actually with much lower values, in graphene films grown on SiO_2 [33]). To this purpose, a very diluted GL water-suspension ($0.1\ \mu\text{g}/\text{mL}$), was used for drop-casting onto mica substrate. Such a low value was chosen in order to prevent the formation of aggregates on the substrate, allowing instead the observation of rather individual GL units. The concentration of water suspension, however, was high enough to allow the presence of a certain number of nanoparticles per unit area of the substrate, so that to be easily detectable in the scanning area of the microscope.

Fig. 5 shows the images collected on this sample, characterized by the presence of nanoparticles deposited on the mica flat surface. A detailed characterization of such particles reveals a size distribution, which can be ascribed to different aggregation amounts of elementary constituents. Selected height profiles crossing the particles demonstrate, first of all, the flatness of the substrate and its suitability for a reliable characterization of the nanoparticles.

From such profiles we observed vertical sizes ranging from about 1 nm or less to few nanometers; the larger lateral dimensions, a few tens of nanometers, confirms that at the chosen concentration of water suspension some aggregations are still occurring (this circumstances also represents an indirect proof that the primary aggregation process occurs to form extended thin planes). These findings support the idea that the elementary units have sub-nanometric vertical size, while their assembling exhibit preferred thickness values.

4. Conclusions

Zeta potential and AFM measurements demonstrate that the quality and the features of the produced self-assembled GL films are strongly affected by the pH of the water suspension from which the films themselves are prepared. The observed morphologic differences are consistent with the interactions features expected for surfaces having different hydrophilic character as a consequence of a different amount of deprotonation of carboxylic groups: the observation of grains or of flat surfaces can be easily understood in terms of consequent surface tension (macroscopic point of view) or, equivalently, in terms of microscopic interaction between the fundamental units in the water suspension. Besides such evident important difference in the quality of films surfaces, the morphological measurements seem to indicate the occurrence of a preferred basic thickness for the assembled layers: this circumstance can be also interpreted in terms of simple fundamental principles based on the forces concurring in a colloidal suspension. Of course, the proposed mechanisms for the observed preferred thickness are suggested hypotheses, which deserve further experimental work to be verified or improved, for example by measuring the films features when varying further preparation parameter. On the other hand, the role of surface tension and of the described microscopic forces in determining the two observed morphological regimes, their relation with the carboxylic groups on the film surface, as well as the fact that the observed layers are formed by smaller fundamental constituents, are well supported by the measured morphology and further experimental observation, and open the way to the possibility to control the surface feature of

GL layers by properly acting on accessible preparation parameters.

Acknowledgments

The work was partially financed by Accordo CNR-MSE “Utilizzo pulito dei combustibili fossili ai fini del risparmio energetico” 2011–2012. The authors greatly acknowledge prof. Carla Manfredi (Dipartimento di Chemistry, Università di Napoli “Federico II”) for coulometric – potentiometric titration. XPS measurements were performed within the proposal 20142026 financed by CERiC-ERIC: “Structural characterization of HKUST-1 intercalated with conductive graphene-like layers”.

References

- [1] A. Dimiev, D.V. Kosynkin, A. Sinitskii, A. Slesarev, Z.Z. Sun, J.M. Tour, *Science* 331 (2011) 1168.
- [2] S. Varghese, S. Das, *J. Phys. Chem. Lett.* 2 (2011) 863.
- [3] C. Wang, H. Dong, W. Hu, Y. Liu, D. Zhu, *Chem. Rev.* 112 (2012) 2208.
- [4] L. Hu, D.S. Hecht, G. Gruner, *Chem. Rev.* 110 (2010) 5790.
- [5] J. Du, S. Pei, L. Ma, H.M. Cheng, *Adv. Mater.* 26 (2014) 1958.
- [6] X. Ou, P. Chen, L. Jiang, Y. Shen, W. Hu, M. Liu, *Adv. Funct. Mater.* 24 (2014) 543.
- [7] M. Inagaki, *Carbon* 50 (2012) 3247.
- [8] R. Hauert, K. Thorwarth, G. Thorwarth, *Surf. Coat. Technol.* 233 (2013) 119.
- [9] D. Zhang, H. Tang, Y. Wang, K. Wu, H. Huang, G. Tang, J. Yang, *Appl. Surf. Sci.* 319 (2014) 306.
- [10] L. Luo, Y. Li, J. Hou, Y. Yang, *Appl. Surf. Sci.* 319 (2014) 332.
- [11] M. Alfè, V. Gargiulo, R. Di Capua, F. Chiarella, J.N. Rouzaud, A. Vergara, A. Cijajolo, *ACS Appl. Mater. Interfaces* 4 (2012) 4491.
- [12] M. Alfè, V. Gargiulo, L. Lisi, R. Di Capua, *Mater. Chem. Phys.* 147 (2014) 744.
- [13] M. Alfè, D. Spasiano, V. Gargiulo, G. Vitiello, R. Di Capua, R. Marotta, *Appl. Catal. A: Gen.* 487 (2014) 91.
- [14] V. Gargiulo, M. Alfè, R. Di Capua, A.R. Togna, V. Cammisotto, S. Fiorito, A. Musto, A. Navarra, S. Parisi, A. Pezzella, *J. Mater. Chem. B* 3 (2015) 5070.
- [15] S. Stankovich, D.A. Dikin, R.D. Piner, K.A. Kohlhaas, A. Kleinhammens, Y. Jia, Y. Wu, S.T. Nguyen, R.S. Ruoff, *Carbon* 45 (2007) 1558.
- [16] S. Visentin, N. Barbero, S. Musso, V. Mussi, C. Biale, R. Ploeger, G. Viscardi, *Chem. Commun.* 46 (2010) 1443.
- [17] E. Carella, M. Ghiazza, M. Alfè, E. Gazzano, D. Ghigo, V. Gargiulo, A. Cijajolo, B. Fubini, I. Fenoglio, *BioNanoSci* 3 (2013) 112.
- [18] G. Gran, *Analyst* 77 (1952) 661.
- [19] L.G. Sillén, B. Warnqvist, *Ark. Kemi* 31 (1969) 315.
- [20] V. Strelko Jr., D.J. Malik, M. Streat, *Carbon* 40 (2002) 95.
- [21] H.F. Gorgulho, J.P. Mesquita, F. Goncalves, M.F.R. Pereira, J.L. Figueiredo, *Carbon* 46 (2008) 1544.
- [22] A.M. Dimiev, L.B. Alemany, J.M. Tour, *ACS Nano* 7 (2013) 576.
- [23] D.H. Everett, *Basic Principles of Colloid Science*, The Royal Society of Chemistry, London, 1988.
- [24] J.I. Paredes, S. Villar-Rodil, P. Solis-Fernandez, A. Martinez-Alonso, J.M.D. Tascon, *Langmuir* 25 (2009) 5957.
- [25] P.G. de Gennes, *Rev. Mod. Phys.* 57 (1985) 827.
- [26] R.D. Deegan, O. Bakajin, T.F. Dupont, G. Huber, S.R. Nagel, T.A. Witten, *Nature* 389 (1997) 827.
- [27] D. Yang, A. Velamakanni, G. Bozoklu, S. Park, M. Stoller, R.D. Piner, S. Stankovich, I. Jung, Da.A. Field, C.A. Ventrone Jr., R.S. Ruoff, *Carbon* 47 (2009) 145.
- [28] S. Yumitori, *J. Mater. Sci.* 35 (2000) 139.
- [29] J.N. Israelachvili, *Intermolecular and Surface Forces*, Academic Press, London, 1992.
- [30] G. Reiter, G.R. Strobl, *Progress in Understanding of Polymer Crystallization*, Springer Verlag, Berlin, 2007.
- [31] K. Armitstead, G. Goldbeck-Wood, A. Keller, *Polymer crystallization theories, in: Macromolecules: Synthesis, Order and Advanced Properties*, *Adv. Polymer Sci.* 100 (1) (1992) 219–312.
- [32] H.J. Butt, K. Graf, M. Kappl, *Physics and Chemistry of Interfaces*, Wiley-VCH, 2013.
- [33] C. Casiraghi, A. Hartschuh, E. Lidorikis, H. Qian, H. Harutyunyan, T. Gokus, K.S. Novoselov, A.C. Ferrari, *Nano Lett.* 7 (2007) 2711.